Research Article Vol. 29, No. 4 / 15 February 2021 / Optics Express 5890
Optics EXPRESS

Controlled unidirectional reflection in cold atoms via the spatial Kramers-Kronig relation

YAN ZHANG,[1] JIN-HUI WU,[1,2,*] M. ARTONI,[3] AND G. C. LA ROCCA[4]

[1]School of Physics, Northeast Normal University, Changchun 130024, China
[2]State Key Laboratory of Quantum Optics and Quantum Optics Devices, Shanxi University, Taiyuan 030006, China
[3]Department of Engineering and Information Technology and Istituto Nazionale di Ottica (INO-CNR), Brescia University, 25133 Brescia, Italy
[4]Scuola Normale Superiore and CNISM, 56126 Pisa, Italy
[*]jhwu@nenu.edu.cn

Abstract: It is known that the Kramers-Kronig (KK) relation between real and imaginary parts of the optical susceptibility in the frequency domain can also be realized in the space domain, as first proposed in [Nat. Photonics **9**(7), 436 (2015)]. We here study a mechanism to implement spatial KK relations in a cold atomic sample and use it to control unidirectional reflectionless for probe light incident from either the left or right side of the sample at will. In our model, the complex frequency dependent atomic susceptibility is mapped into a spatially dependent one, employing a far-detuned driving field of intensity linearly varied in space. The reflection of an incident light from one side of the sample can then be set to vanish over a specific frequency band directly by changing the driving field parameters, such as its intensity and frequency. Also, by incorporating the Bragg scattering into the spatial KK relation, the reflectivity from the opposite side of the sample, though typically small for realistic atomic densities, can be made to increase to improve the reflectivity contrast. The present scheme bears potentials for all-optical network applications that require controllable unidirectional light propagation.

1. Introduction

Asymmetric reflection control of the flow of a light beam is a key technique to perform photonic and quantum communication manipulations. Unidirectional reflectionless, in particular, has attracted much research efforts because of its perspective applications in developing novel photonic devices [1–9]. Control over reflection of a light beam incident from opposite sides of a device is usually reciprocal and static, *i.e.*, takes place with identical reflectivity values and cannot be changed. This can be achieved, *e.g.*, using photonic band-gap materials exhibiting a given periodic structure of the real refractive index [10,11]. Tunable photonic band gap structures have also been proven to be viable, where control of the periodic structure of the complex susceptibility can be done, e.g., through electromagnetically induced transparency (EIT) [12–14], with homogeneous atomic clouds dressed by standing-wave coupling fields [15–22] or periodic atomic lattices dressed by traveling-wave coupling fields [23–33]. Generally speaking, it is hard to achieve asymmetric light transport through standard linear optical processes [34–36], though significant progresses have been made recently in coherently driven moving atomic lattices [1,2,32] and in materials exhibiting parity-time (PT) symmetry or asymmetry [3,4,37–41]. Realistic implementations of these schemes are challenging owing to complex atom-light coupling configurations, precise light field arrangement in space and peculiar balanced gain and loss over a single period.

Alternatively, asymmetric and unidirectional reflection can be realized in an inhomogeneous continuous medium as the usual Kramers-Kronig (KK) relation, satisfied by its complex optical

#415879 https://doi.org/10.1364/OE.415879
Journal © 2021 Received 27 Nov 2020; revised 14 Jan 2021; accepted 19 Jan 2021; published 9 Feb 2021

Optics EXPRESS

response function, is mapped from the frequency domain to the space domain [5–8,42–49]. In the pioneering work [5], Horsley *et al.* found that a non-Hermitian medium would not reflect light from one side for all incident angles if its complex permittivity satisfies the spatial KK relation, which promises also the realization of omnidirectional perfect absorber [7] and media with no transmission [50]. When extended into discrete lattices, complex potentials exhibiting the spatial KK relation may further become invisible to support a bidirectional reflectionless behavior [48,49]. Notice, in addition, that the original idea has been already experimentally demonstrated via a suitable design of different inhomogeneous media [7,43,51,52]. All above findings not only deepen our understanding of light propagation, but also provide new platforms toward multi-functional optical elements, especially those requiring perfect antireflection properties. Yet, schemes so far studied rely on fixed complex refractive index, susceptibility, or permittivity structures and hence lack of dynamic tunability.

Here we propose an efficient scheme for mapping the KK relation of a probe susceptibility from the frequency domain into the space domain in a cold atomic sample. The scheme hinges on devising a position-dependent ground level shift with a far detuned external control field whose intensity can be linearly varied in space (see Sect. 2). Other spatially dependent EIT systems have also been used to manipulate structured light beams, albeit via phase-dependent dark-states [53–55]. It is worth noting that in our scheme, depending on the probe frequency, spatial KK relations may be completely or partially fulfilled or even destroyed; in the following these are termed respectively as "unbroken", "transitional", and "broken" regimes. The unbroken regime is of particular interest here because it enables us to attain reflectionless manipulation of a probe beam incident on one sample end over a tunable range of frequencies. The transitional regime may instead be exploited to attain reflectionless manipulation from both sample side ends, albeit at different frequencies. Furthermore, changing the "sign" of the ground level shift enables us to directly swap the direction of the vanishing reflectivity whereas increasing the level shift "magnitude" leads to an enhancement of the nonzero reflectivity while maintaining (on the other side) a vanishing reflectivity. Bragg scattering may also be incorporated into the spatial KK relation to further increase the forward-backward reflectivity contrast.

2. Model and equations

We consider in Fig. 1(a) a cold atomic sample extending from $x = 0$ to $x = L$, driven by a weak probe field of amplitude (frequency) $\mathbf{E}_p$ (ω_p) and a strong control field of amplitude (frequency) $\mathbf{E}_c$ (ω_c). The control field is assumed to illuminate the sample along the $-y$ direction while the probe field can travel through the sample along either x or $-x$ direction. All atoms are driven into the three-level V configuration, as shown in Fig. 1(b), characterized by Rabi frequencies (detunings) $\Omega_p = \mathbf{E}_p \cdot \mathbf{d}_{ge}/2\hbar$ on transition $|g\rangle \leftrightarrow |e\rangle$ ($\Delta_p = \omega_p - \omega_{eg}$) and $\Omega_c = \mathbf{E}_c \cdot \mathbf{d}_{ga}/2\hbar$ on transition $|g\rangle \leftrightarrow |a\rangle$ ($\Delta_c = \omega_c - \omega_{ag}$), being $\mathbf{d}_{\mu\nu}$ and $\omega_{\mu\nu}$ dipole moments and resonant frequencies of relevant transitions. We have also used Γ_{ag} and Γ_{eg} to describe the population decay rates from levels $|a\rangle$ and $|e\rangle$ to level $|g\rangle$, respectively. To be more concrete, levels $|a\rangle$, $|e\rangle$, and $|g\rangle$ may refer to states $|5P_{3/2}, F = 3, m_F = 3\rangle$, $|5P_{1/2}, F = 1, m_F = 1\rangle$, and $|5S_{1/2}, F = 2, m_F = 2\rangle$ of ^{87}Rb atoms, respectively. This choice ensures that (*i*) dipole moments $|\mathbf{d}_{ge}|$ and $|\mathbf{d}_{ga}|$ take the largest possible values, which could relax the requirement of a very dense atomic sample for achieving a high reflectivity contrast; (*ii*) the control field doesn't couple level $|g\rangle$ to a fourth level even in the case of a large $|\Delta_c|$, because no others except level $|a\rangle$ has $m_F = 3$ on the D_2 line of ^{87}Rb atoms. Most importantly, we will assume that the control field is linearly varied in intensity along the x direction, *e.g.*, by a neutral density filter (NDF). In this case, $|\Omega_c|^2$ should be replaced by $|\Omega_c(x)|^2 = x|\Omega_{c0}|^2/L$ with Ω_{c0} denoting the maximal Rabi frequency at $x = L$.

With the electric-dipole and rotating-wave approximations, working in the weak probe limit, we can solve density matrix equations for the three-level V configuration to attain the steady-state

Optics EXPRESS

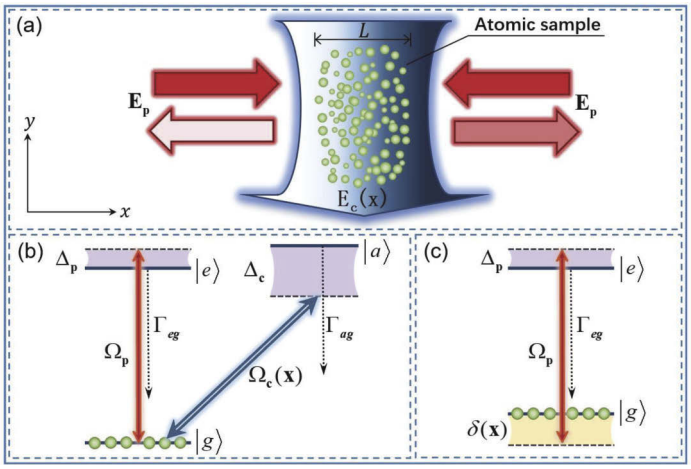

Fig. 1. (a) A cold atomic sample illuminated by a control beam $\mathbf{E}_c(x)$ along the $-y$ direction exhibits a strongly asymmetric reflection for a probe beam $\mathbf{E}_p$ incident either along the $+x$ or the $-x$ direction. (b) A three-level atomic system driven by a probe field of Rabi frequency Ω_p (detuning Δ_p) and a control field of Rabi frequency $\Omega_c(x)$ (detuning Δ_c) into the V configuration. (c) A two-level atomic system with a dynamic shift $\delta(x)$ of level $|g\rangle$ upon the adiabatic elimination of level $|a\rangle$.

probe susceptibility

$$\chi_3(\Delta_p, x) = i\frac{N_0|\mathbf{d}_{ge}|^2}{\varepsilon_0\hbar}\frac{[(\gamma_{ga}^2+\Delta_c^2)+|\Omega_c(x)|^2][\gamma_{ea}-i(\Delta_c-\Delta_p)]-|\Omega_c(x)|^2(\gamma_{ga}-i\Delta_c)}{[(\gamma_{ga}^2+\Delta_c^2)+|\Omega_c(x)|^2]\{[\gamma_{ea}-i(\Delta_c-\Delta_p)](\gamma_{ge}-i\Delta_p)+|\Omega_c(x)|^2\}}, \quad (1)$$

where N_0 denotes the homogeneous atomic density while $\gamma_{\mu\nu}$ is the coherence dephasing rate on transition $|\mu\rangle \leftrightarrow |\nu\rangle$ with $\gamma_{ge} = \Gamma_{eg}/2$, $\gamma_{ga} = \Gamma_{ag}/2$, and $\gamma_{ea} = (\Gamma_{ag}+\Gamma_{eg})/2$. Now we consider that the control field is far detuned from transition $|g\rangle \leftrightarrow |a\rangle$ by requiring $\Delta_c \gg \Omega_{c0}, \gamma_{ga}$. In this case, level $|a\rangle$ can be adiabatically eliminated from the three-level V configuration to yield a two-level system [see Fig. 1(c)], in which level $|g\rangle$ suffers a position-dependent energy shift $\delta(x) = |\Omega_c(x)|^2/\Delta_c = x\delta_0/L$ with $\delta_0 = |\Omega_{c0}|^2/\Delta_c$. Then the probe susceptibility can be cast into a more compact form as given by

$$\chi_2(\Delta_p, x) = i\frac{N_0|\mathbf{d}_{ge}|^2}{\varepsilon_0\hbar}\frac{1}{\gamma_{ge}-i[\Delta_p+\delta(x)]}, \quad (2)$$

whose real (χ_2') and imaginary (χ_2'') parts govern the *local* dispersive and absorption properties around the probe resonance, respectively. The possibility to control the effective detuning $\Delta_p^{eff}(x) = \Delta_p + \delta(x)$ by changing the ground level shift $\delta(x)$ amounts to a direct mapping from the spatially linear variation of the control intensity to that of the probe detuning.

The real and imaginary parts of χ_2 are well known to be related via the KK relation in the frequency domain based on the causality principle and Cauchy's theorem if we set $\delta(x) \equiv 0$ [56]. Thus, for appropriate probe detunings and sufficiently long samples such that the spatial variation of the effective probe detuning induced by $\delta(x)$ is fully developed, as shown by the red solid lines in Figs. 2(a) and 2(b), the KK relation holds in the space domain and can be defined by the following Cauchy's principal value integral

$$\chi_2'(\Delta_p, x) = \frac{1}{\pi}\mathrm{P}\int_0^L \frac{\chi_2''(\Delta_p, s)}{s-x}ds \quad (3)$$

Optics EXPRESS

over spatial coordinate s along the x direction, where P indicates the principal part of the integral after excluding the singular point $s = x$.

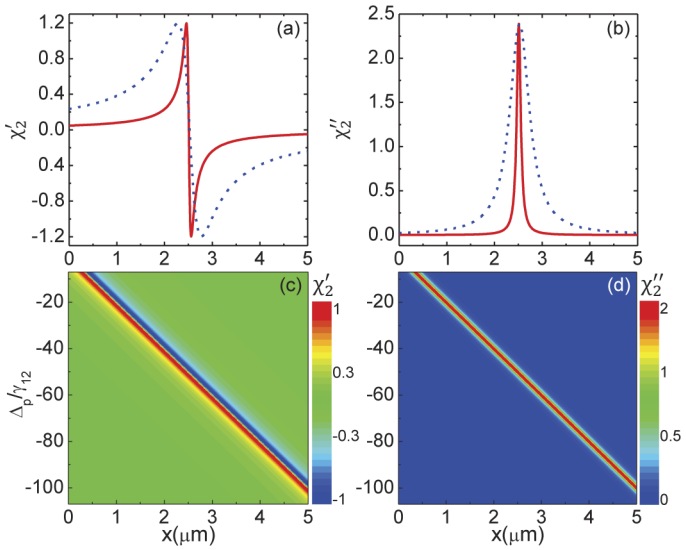

Fig. 2. (a) Real and (b) imaginary parts of susceptibility χ_2 against position x with δ_0/γ_{ge}=100 and $\Delta_p/\gamma_{ge} = -50$ (red-solid); δ_0/γ_{ge}=20 and $\Delta_p/\gamma_{ge} = -10$ (blue-dashed). (c) Real and (d) imaginary parts of susceptibility χ_2 against position x and detuning Δ_p with δ_0/γ_{ge}=100. Other parameters used in calculations are $\gamma_{ge} = 2\pi \times 2.87$ MHz, $d_{ge} = 1.79 \times 10^{-29}$ C·m, $N_0 = 2.0 \times 10^{13}$ cm^{-3}, $L = 5.0$ μm, and $\lambda_p = 795$ nm.

A medium described by χ_2 in Eq. (2) is expected to exhibit asymmetric light transport features, which can be examined via the standard transfer-matrix method [57–59] as sketched below. First, the atomic sample is partitioned along the x direction into a large number (J) of slices labeled by $j \in [1, J]$, which exhibit slightly different susceptibilities $\bar{\chi}_j(\Delta_p) = \chi_2(\Delta_p, jl)$ but identical length $l = L/J = 10$ nm. Second, a 2×2 unimodular transfer matrix $M_j(\Delta_p, l)$ characterized by l and $\bar{\chi}_j(\Delta_p)$ can be established to describe the propagation of an incident probe field of wavelength λ_p through the *jth* slice by

$$\begin{bmatrix} E_p^+(\Delta_p, jl) \\ E_p^-(\Delta_p, jl) \end{bmatrix} = M_j(\Delta_p, l) \begin{bmatrix} E_p^+(\Delta_p, jl - l) \\ E_p^-(\Delta_p, jl - l) \end{bmatrix}, \tag{4}$$

where E_p^+ and E_p^- denote the forward and backward components of the probe field, respectively. Third, the total transfer matrix of the atomic sample turns out to be $M(\Delta_p, L) = M_J(\Delta_p, l) \cdots M_j(\Delta_p, l) \cdots M_1(\Delta_p, l)$ as a multiplication of the individual transfer matrices of all atomic slices. Finally, we can write the reflectivities ($R_l \neq R_r$) and the transmissivities ($T = T_l = T_r$) as

$$\begin{aligned} R_l(\Delta_p, L) &= \left|r_l(\Delta_p, L)\right|^2 = \left|\frac{M_{(21)}(\Delta_p, L)}{M_{(22)}(\Delta_p, L)}\right|^2, \\ R_r(\Delta_p, L) &= \left|r_r(\Delta_p, L)\right|^2 = \left|\frac{M_{(12)}(\Delta_p, L)}{M_{(22)}(\Delta_p, L)}\right|^2, \\ T(\Delta_p, L) &= \left|t(\Delta_p, L)\right|^2 = \left|\frac{1}{M_{(22)}(\Delta_p, L)}\right|^2 \end{aligned} \tag{5}$$

Optics EXPRESS

in terms of the four matrix elements of $M(\Delta_p, L)$. Here the subscripts 'l' and 'r' have been used to denote that the weak probe field is incident from the left and right sides along the x and $-x$ directions, respectively.

3. Results and discussion

In this section, we show via numerical calculations how to implement the spatial KK relation in a narrow spectral range by tailoring the complex probe susceptibility, and how to implement the unidirectional reflection of a high reflectivity contrast by utilizing the spatial KK relation. All numerical calculations will be done with realistic parameters corresponding to the three states of ^{87}Rb atoms chosen above, though our driving configuration can also be realized, *e.g.*, in other alkali metal atoms.

First, we plot in Figs. 2(a) and 2(b), respectively, the real and imaginary parts of χ_2 against position x for two sets of parameters making the choice $\Delta_p = -\delta_0/2$, which allows the effective probe detuning $\Delta_p^{eff}(x)$ to be in the range of $\{-\delta_0/2, \delta_0/2\}$. It is clear that χ_2' and χ_2'' show an odd profile and an even profile, respectively, centered at $z = L/2$ and practically fully contained by the atomic sample, so they should satisfy the spatial KK relation described by Eq. (3). We also can see that smaller (larger) values of δ_0/γ_{12}, a key dimensionless parameter in our reduced two-level system, will result in broader (narrower) spatial profiles of χ_2' and χ_2'' yet without changing their peak amplitudes. To reveal the frequency-dependent feature, we plot in Figs. 2(c) and 2(d), respectively, the real and imaginary parts of χ_2 against both position x and detuning Δ_p instead. The profiles of χ_2' and χ_2'' are found to move simultaneously toward the left (right) sample end with the increasing (decreasing) of Δ_p. Accordingly, the spatial KK relation will be gradually destroyed because Eq. (3) becomes less and less satisfied.

In order to assess the extent to which the spatial KK relation is satisfied for different probe detunings in a finite atomic sample, here we propose the following integral

$$D_{kk}(\Delta_p) = \frac{\int_0^L \left\{\chi_2'(\Delta_p, x) - \frac{1}{\pi}\mathrm{P}\int_0^L \frac{\chi_2''(\Delta_p, s)}{s-x} ds\right\} dx}{\left|\int_0^L \chi_2'(\Delta_p, x) dx\right|} \tag{6}$$

as a figure of merit for the spatial KK relation. In this definition, $D_{kk} = 0$ denotes the unbroken regime where the spatial KK relation is fully satisfied while $D_{kk} = \pm 1$ denote the broken regime where the spatial KK relation is fully destroyed. According to Eq. (2) and Fig. 2, the spatial profiles of χ_2' and χ_2'' are well contained within our finite atomic sample only for a small range of Δ_p, so the validity of the spatial KK relation is expected to increasingly deteriorate ($D_{kk} = 0 \rightarrow D_{kk} = \pm 1$) as Δ_p is gradually modulated out of this range. This is different from all previous works on spatial KK relation [5–8,42–49], where the susceptibility or permittivity has been assumed to be fixed by design, *i.e.* not tunable.

Then we plot in Fig. 3(a) the reflection and transmission spectra for the parameters used in Figs. 2(a) and 2(b) based on Eq. (5). It is easy to see that these spectra can be divided into three regions: (*I*) where we have $R_l = R_r \rightarrow 0$ and $T \rightarrow 1$; (*II*) where $R_l \neq R_r$ and T are sensitive to Δ_p; (*III*) where $T \simeq 0.05$, $R_l \rightarrow 0$, but R_r oscillates around 0.2. The generation of three different regions can be understood by examining in Fig. 3(b) the figure of merit D_{kk} against probe detuning Δ_p, which clearly shows, as compared to Fig. 3(a), that D_{kk} governs the relation between R_l, R_r, and T. The symmetric (*I*), asymmetric (*II*), and unidirectional (*III*) reflection regions correspond, respectively, to the broken ($D_{kk} = \pm 1$), transitional ($0 < |D_{kk}| < 1$), and unbroken ($D_{kk} = 0$) regimes, and to the cases when the absorption (χ_2'') and dispersion (χ_2') profiles move out of the sample, lie at the sample boundaries, and are well contained by the sample. It is worth noting that in region (*III*) a left (right) incident probe beam is reflectionless (partially reflected) because it first sees the negative (positive) peak of χ_2' [5], and the resonant absorption (χ_2'') is

Optics EXPRESS

already strong enough to yield $T \to 0.0$ for forward photons while the dispersion profile (χ_2') is not too sharp to yield $R_r \to 1.0$ for backward photons. One way for further reducing T and simultaneously increasing R_r is to produce enhanced absorption profiles and sharper dispersion profiles in denser atomic samples. The restricted range of densities of cold atoms available in experiment, however, places a constraint on this approach.

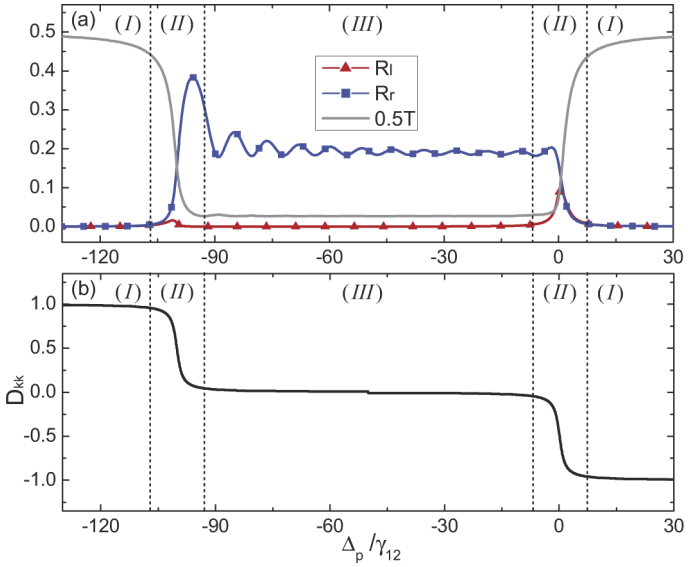

Fig. 3. (a) Reflectivity R_l, reflectivity R_r, and half transmissivity T; (b) figure of merit D_{kk} against detuning Δ_p. Other parameters used in calculations are the same as in Fig. 2(a,b).

Figure 4(a) further shows the different regimes on a diagram with D_{kk} plotted against δ_0 and Δ_p, in which the green region ($D_{kk} = -1$) and the red region ($D_{kk} = 1$) refer to the broken regime (I); the four narrow blue regions ($0<|D_{kk}|<1$) refer to the transitional regime (II); the two triangular yellow regions ($D_{kk} = 0$) refer to the unbroken regime (III). It is also clear that the widths of two yellow regions depend critically on the magnitude of δ_0; a broken regime may be converted into an unbroken regime and vice versa for a given Δ_p by changing the sign of δ_0. Accordingly, it is viable to enlarge or reduce the reflectionless frequency band by varying the magnitude of δ_0 and convert the sample from left reflectionless to right reflectionless or vice versa by changing the sign of δ_0. This potentially dynamic controllability, a chief feature of our proposal, is well demonstrated in Figs. 4(b) and 4(c) in terms of reflectivities R_l and R_r.

It is also interesting to examine what could happen for reflectivities R_l and R_r when sample length L is multiplied while atomic density N_0 remains invariant. In this case, we can see from $\delta(x) = x\delta_0/L$ that the linear variation occurs in a much larger range while its magnitude δ_0 is unchanged. Then, as shown in Fig. 5, the spatially wider/smoother dispersion (χ_2') and absorption (χ_2''), of L-independent maxima and minima, together result in a notable reduction of R_r while R_l remains vanishing in the unbroken regime. The peak of R_l (R_r) accompanied by $R_r \to 0$ ($R_l \to 0$) in the transitional regime has a L-independent position because it only appears as the main profiles of $\chi_2'(x)$ and $\chi_2''(x)$ approach and even partially leave the left (right) sample end. It is clearly not a result of the spatial KK relation and allows two probe beams of different frequencies to be simultaneously reflected or not when they are incident upon the opposite sample ends. The damped oscillations of R_r against Δ_p in the unbroken regime can be understood as a multiple interference effect due to the discontinuities of the probe susceptibility at the right sample end and at the resonant position inside the sample. It is clear that stronger (weaker) oscillations occur

Optics EXPRESS

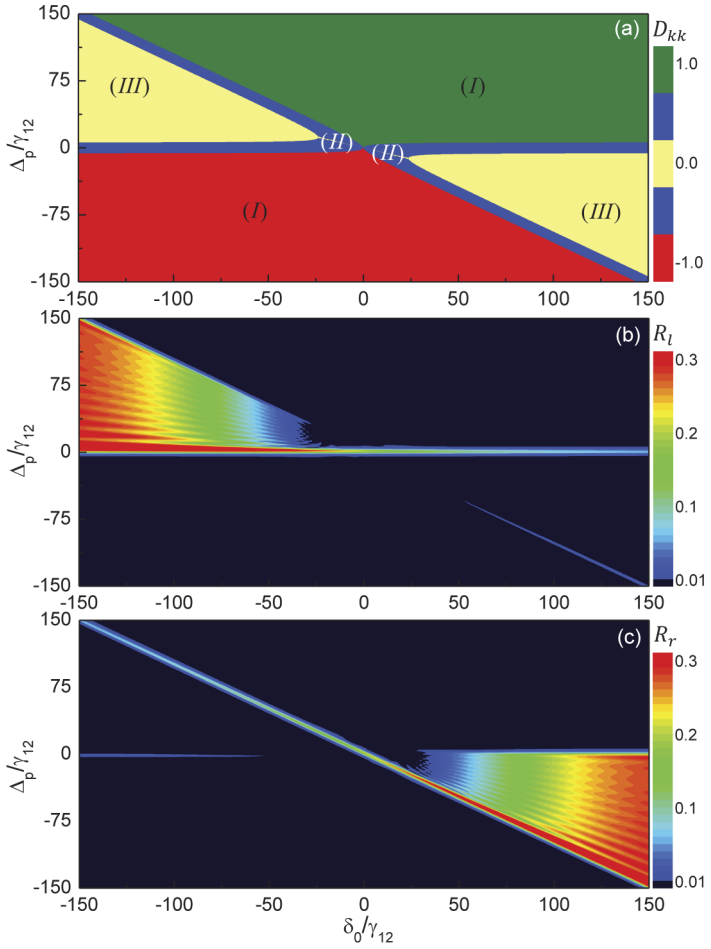

Fig. 4. (a) Figure of merit D_{kk}, (b) reflectivity R_l, and (c) reflectivity R_r (c) against shift δ_0 and detuning Δ_p. Other parameters used in calculations are the same as in Figs. 2(a) and (b).

at larger (smaller) values of $|\Delta_p|$ because the resonant position of $\chi_2'(x)$ and $\chi_2''(x)$ is close to (far from) the right sample end, yielding thus stronger (weaker) discontinuities. The oscillation period can be roughly estimated as $d\Delta_p \simeq \delta_0/L \cdot \lambda_p/2$ by considering that the interval $d\Delta_p$ of two adjacent maxima corresponds to a 2π phase shift ($\lambda_p/2$ spatial shift) gained by the reflected photons ($\chi_2'(x)$ and $\chi_2''(x)$).

Finally, we note that an experiment may typically have a lower atomic density and a larger sample length than in simulations presented so far. To overcome this difficulty, we need to find an alternative way to enhance the nonzero reflectivity in the unbroken regime. This can be done by loading cold atoms into a 1D optical lattice to create a spatially periodic density $N_j(x)$ as described in the caption of Fig. 6, yielding thus Bragg scattering incorporated into the spatial KK relation. As shown in Fig. 6(a) and Fig. 6(b), both dispersion $\chi_2'(x)$ and absorption $\chi_2''(x)$ of one-order lower values now exhibit the comb-like spatial profiles while satisfying to a less extent the spatial KK relation. In this case, we can find from Fig. 6(c) that R_l and R_r are strongly asymmetric in a much smaller frequency range, *e.g.*, with R_r exhibiting a maximal value up to 0.54 while $R_l \lesssim 0.01$ for $-25.5 \lesssim \Delta_p/\gamma_{ge} \lesssim -11.0$. Figure 6(d) further shows that the reflectivity contrast $C = (R_r - R_l)/(R_r + R_l)$, an important figure of merit on the asymmetric reflection, could

Optics EXPRESS

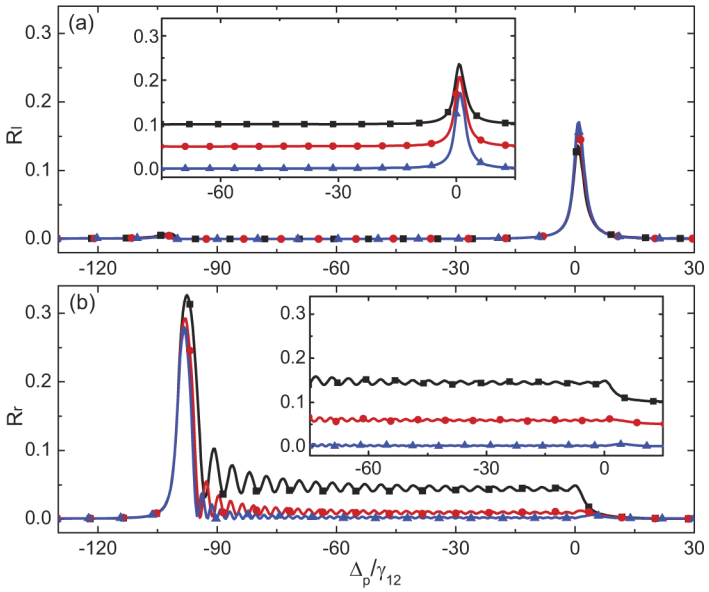

Fig. 5. Reflectivities (a) R_l and (b) R_r against detuning Δ_p for $L = 10$ μm (black-squares), $L = 15$ μm (red-circles), and $L = 20$ μm (blue-triangles). Other parameters used in calculations are the same as in Figs. 2(a) and (b). Black (red) curves are shown with a vertical offset 0.1 (0.05) in both insets.

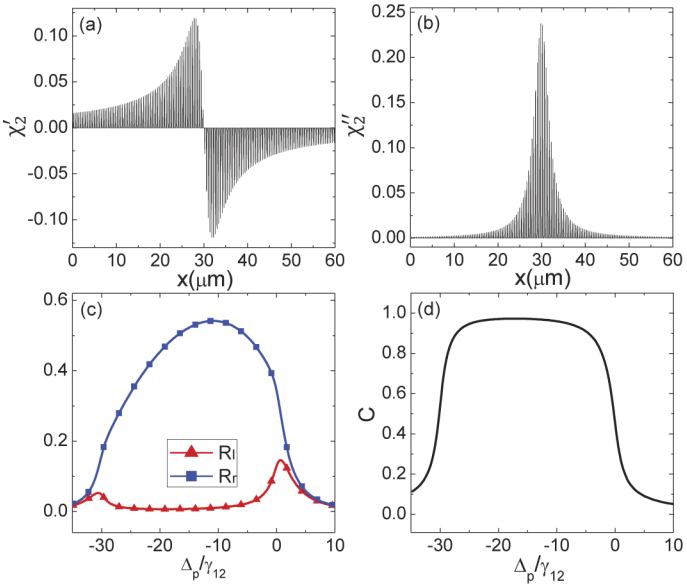

Fig. 6. Spatial profiles of (a) χ_2' and (b) χ_2'' as well as corresponding spectra of (c) reflectivities $R_{l,r}$ and (d) contrast C for an atomic lattice of density $N_j(x) = N_0 e^{-(x-x_j)^2/\delta x^2}$ in the *jth* trap of center $x_j = (j - 1/2)\Lambda$, width δx, and period Λ. Parameters are the same as in Fig. 2(b) except $N_0 = 2.0 \times 10^{12}$ cm^{-3}, $L = 60$ μm, $\delta_0/\gamma_{ge} = 30$, $\Lambda = 400$ nm, and $\delta x = \Lambda/6$.

Optics EXPRESS

be up to 0.97 and is over 0.90 for $-27.0 \lesssim \Delta_p/\gamma_{ge} \lesssim -4.5$. It is noticeable that the incorporation of Bragg scattering, typically yielding symmetric reflectivities, has negligible effects on the vanishing reflectivity but largely enhances the nonzero reflectivity and the reflectivity contrast. That means, replacing a constant density N_0 with a periodic density $N_j(x)$ does not hamper the implementation of spatial KK relation, which is essential for developing nonreciprocal optical devices requiring a high reflectivity contrast.

It has been shown that atoms could be trapped and guided using nanofabricated wires and surfaces to form atom chips [60]. These chips provide a versatile experimental platform with cold atoms and constitute the basis for wide and robust applications ranging from atom optics to quantum optics. They have been used, for instance, in diverse experiments involving quantum simulation, metrology, and information processing [61–63]. We then believe that our proposal is well poised to atom-chip implementations in integrated optical devices.

4. Conclusions

In summary, we have investigated the spatial KK relation and relevant reflection features in a short and dense sample of cold ^{87}Rb atoms. This nontrivial relation in regard of the probe susceptibility is enabled by generating a position-dependent ground level shift $\delta(x)$ with a far detuned control field of intensity linearly varied along the x direction. We find, in particular, that the figure of merit D_{kk} characterizing the spatial KK relation may switch from the unbroken regime of unidirectional reflection, via the transitional regime of asymmetric reflection, to the broken regime of symmetric reflection, or vice versa. This is attained by increasing the maximal level shift δ_0 from a negative value to a positive value or considering an inverse process, depending on the sign of probe detuning Δ_p. A swapping between the nonzero reflectivity and the vanishing reflectivity at opposite sample ends is also viable by changing the sign of maximal level shift δ_0. It is of more interest that the nonzero reflectivity can be well enhanced to result in a high reflectivity contrast for lower densities and larger lengths in a cold atomic lattice, indicating that Bragg scattering does not hamper or spoil the main effects of spatial KK relation. Such a feasible scheme may inspire further applications in nonreciprocal optical devices and provide a promising platform for atom-chip implementations.

Funding. National Natural Science Foundation of China (11534002, 11674049, 11704064, 11861131001); Ministero degli Affari Esteri e della Cooperazione Internazionale (PGR00960); Program of State Key Laboratory of Quantum Optics and Quantum Optics Devices (KF201807); Fundamental Research Funds for the Central Universities (2412019FZ045).

Disclosures. The authors declare that there are no conflicts of interest related to this article.

References

1. D.-W. Wang, H.-T. Zhou, M.-J. Guo, J. X. Zhang, J. Evers, and S.-Y. Zhu, "Optical diode made from a moving photonic crystal," Phys. Rev. Lett. **110**(9), 093901 (2013).
2. S. A. R. Horsley, J.-H. Wu, M. Artoni, and G. C. La Rocca, "Optical nonreciprocity of cold atom bragg mirrors in motion," Phys. Rev. Lett. **110**(22), 223602 (2013).
3. J.-H. Wu, M. Artoni, and G. C. La Rocca, "Non-Hermitian degeneracies and unidirectional reflectionless atomic lattices," Phys. Rev. Lett. **113**(12), 123004 (2014).
4. J.-H. Wu, M. Artoni, and G. C. La Rocca, "Parity-time-antisymmetric atomic lattices without gain," Phys. Rev. A **91**(3), 033811 (2015).
5. S. A. R. Horsley, M. Artoni, and G. C. La Rocca, "Spatial Kramers-Kronig relations and the reflection of waves," Nat. Photonics **9**(7), 436–439 (2015).
6. S. Longhi, "Bidirectional invisibility in Kramers-Kronig optical media," Opt. Lett. **41**(16), 3727–3730 (2016).
7. W. Jiang, Y. Ma, J. Yuan, G. Yin, W. Wu, and S. He, "Deformable broadband metamaterial absorbers engineered with an analytical spatial Kramers-Kronig permittivity profile," Laser Photonics Rev. **11**(1), 1600253 (2017).
8. S. A. R. Horsley and S. Longhi, "Spatiotemporal deformations of reflectionless potentials," Phys. Rev. A **96**(2), 023841 (2017).
9. A. Calabrese, F. Ramiro-Manzano, H. M. Price, S. Biasi, M. Bernard, M. Ghulinyan, I. Carusotto, and L. Pavesi, "Unidirectional reflection from an integrated taiji microresonator," Photonics Res. **8**(8), 1333–1341 (2020).
10. S. John, "Strong localization of photons in certain disordered dielectric superlattices," Phys. Rev. Lett. **58**(23), 2486–2489 (1987).

Optics EXPRESS

11. K. Sakoda, *Optical properties of photonic crystals* (Springer, 2001).
12. S. E. Harris, "Electromagnetically induced transparency," Phys. Today **50**(7), 36–42 (1997).
13. M. Fleischhauer, A. Imamoglu, and J. P. Marangos, "Electromagnetically induced transparency: Optics in coherent media," Rev. Mod. Phys. **77**(2), 633–673 (2005).
14. N. Kukharchyk, D. Sholokhov, O. Morozov, S. L. Korableva, A. A. Kalachev, and P. A. Bushev, "Electromagnetically induced transparency in a mono-isotopic 167Er:7LiYF4 crystal below 1 Kelvin: microwave photonics approach," Opt. Express **28**(20), 29166–29177 (2020).
15. A. André and M. D. Lukin, "Manipulating light pulses via dynamically controlled photonic band gap," Phys. Rev. Lett. **89**(14), 143602 (2002).
16. X.-M. Su and B. S. Ham, "Dynamic control of the photonic band gap using quantum coherence," Phys. Rev. A **71**(1), 013821 (2005).
17. M. Artoni and G. C. La Rocca, "Optically tunable photonic stop bands in homogeneous absorbing media," Phys. Rev. Lett. **96**(7), 073905 (2006).
18. J. Wu, Y. Liu, D.-S. Ding, Z.-Y. Zhou, B.-S. Shi, and G. C. Guo, "Light storage based on four-wave mixing and electromagnetically induced transparency in cold atoms," Phys. Rev. A **87**(1), 013845 (2013).
19. Y. Zhang, Y.-M. Liu, X.-D. Tian, T.-Y. Zheng, and J.-H. Wu, "Tunable high-order photonic band gaps of ultraviolet light in cold atoms," Phys. Rev. A **91**(1), 013826 (2015).
20. D.-W. Wang, H. Cai, L. Yuan, S.-Y. Zhu, and R.-B. Liu, "Topological phase transitions in superradiance lattices," Optica **2**(8), 712–715 (2015).
21. F. Wen, H. Ye, X. Zhang, W. Wang, S. Li, H. Wang, Y. Zhang, and C. Qiu, "Optically induced atomic lattice with tunable near-field and far-field diffraction patterns," Photonics Res. **5**(6), 676–683 (2017).
22. H. Yang, T. Zhang, Y. Zhang, and J.-H. Wu, "Dynamically tunable three-color reflections immune to disorder in optical lattices with trapped cold ^{87}Rb atoms," Phys. Rev. A **101**(5), 053856 (2020).
23. G. Birkl, M. Gatzke, I. H. Deutsch, S. L. Rolston, and W. D. Phillips, "Bragg scattering from atoms in optical lattices," Phys. Rev. Lett. **75**(15), 2823–2826 (1995).
24. I. H. Deutsch, R. J. C. Spreeuw, S. L. Rolston, and W. D. Phillips, "Photonic band gaps in optical lattices," Phys. Rev. A **52**(2), 1394–1410 (1995).
25. P. M. Visser and G. Nienhuis, "Band gaps and group velocity in optical lattices," Opt. Commun. **136**(5-6), 470–479 (1997).
26. S. Slama, C. von Cube, M. Kohler, C. Zimmermann, and P. W. Courteille, "Multiple reflections and diffuse scattering in Bragg scattering at optical lattices," Phys. Rev. A **73**(2), 023424 (2006).
27. M. Antezza and Y. Castin, "Fano-Hopfield model and photonic band gaps for an arbitrary atomic lattice," Phys. Rev. A **80**(1), 013816 (2009).
28. A. Schilke, C. Zimmermann, P. W. Courteille, and W. Guerin, "Photonic band gaps in one-dimensionally ordered cold atomic vapors," Phys. Rev. Lett. **106**(22), 223903 (2011).
29. D. Petrosyan, "Tunable photonic band gaps with coherently driven atoms in optical lattices," Phys. Rev. A **76**(5), 053823 (2007).
30. D. Yu, "Photonic band structure of the three-dimensional ^{88}Sr atomic lattice," Phys. Rev. A **84**(4), 043833 (2011).
31. A. Schilke, C. Zimmermann, and W. Guerin, "Photonic properties of one-dimensionally-ordered cold atomic vapors under conditions of electromagnetically induced transparency," Phys. Rev. A **86**(2), 023809 (2012).
32. L. Yang, Y. Zhang, X.-B. Yan, Y. Sheng, C.-L. Cui, and J.-H. Wu, "Dynamically induced two-color nonreciprocity in a tripod system of a moving atomic lattice," Phys. Rev. A **92**(5), 053859 (2015).
33. Y. Zhang, Y.-M. Liu, T.-Y. Zheng, and J.-H. Wu, "Light reflector, amplifier, and splitter based on gain-assisted photonic band gaps," Phys. Rev. A **94**(1), 013836 (2016).
34. P. Yeh, *Optical Waves in Layered Media* (Wiley-Interscience, 2005).
35. L. Chang, X. Jiang, S. Hua, C. Yang, J. Wen, L. Jiang, G. Li, G. Wang, and X. Min, "Parity-time symmetry and variable optical isolation in active-passive-coupled microresonators," Nat. Photonics **8**(7), 524–529 (2014).
36. B. Peng, S. K. Özdemir, F. Lei, F. Monifi, M. Gianfreda, G. L. Long, S. Fan, F. Nori, C. M. Bender, and L. Yang, "Parity-time-symmetric whispering-gallery microcavities," Nat. Phys. **10**(5), 394–398 (2014).
37. Z. Lin, H. Ramezani, T. Eichelkraut, T. Kottos, H. Cao, and D. N. Christodoulides, "Unidirectional invisibility induced by PT-symmetric periodic structures," Phys. Rev. Lett. **106**(21), 213901 (2011).
38. L. Feng, Y.-L. Xu, W. S. Fegadolli, M.-H. Lu, J. E. B. Oliveira, V. R. Almeida, Y.-F. Chen, and A. Scherer, "Experimental demonstration of a unidirectional reflectionless parity-time metamaterial at optical frequencies," Nat. Mater. **12**(2), 108–113 (2013).
39. X. Wang and J. -H. Wu, "Optical PT-symmetry and PT-antisymmetry in coherently driven atomic lattices," Opt. Express **24**(4), 4289–4298 (2016).
40. S. K. Gupta, Y. Zou, X.-Y. Zhu, M.-H. Lu, L.-J. Zhang, X.-P. Liu, and Y.-F. Chen, "Parity-Time Symmetry in Non-Hermitian Complex Optical Media," Adv. Mater. **32**, 1903639 (2019).
41. Yuan Lijun and Yan Lu Ya, "Unidirectional reflectionless transmission for two-dimensional PT-symmetric periodic structures," Phys. Rev. A **100**(5), 053805 (2019).
42. A. Akyurtlu and A.-G. Kussow, "Relationship between the Kramers-Kronig relations and negative index of refraction," Phys. Rev. A **82**(5), 055802 (2010).

Optics EXPRESS

43. D. Ye, C. Cao, T. Zhou, and J. Huangfu, "G. Zheng and L. Ran, Observation of reflectionless absorption due to spatial Kramers-Kronig profile," Nat. Commun. **8**(1), 51 (2017).
44. S. Longhi, "Wave reflection in dielectric media obeying spatial Kramers-Kronig relations," EPL **112**(6), 64001 (2015).
45. T. G. Philbin, "All-frequency reflectionlessness," J. Opt. **18**(1), 01LT01 (2016).
46. S. A. R. Horsley, M. Artoni, and G. C. La Rocca, "Reflection of waves from slowly decaying complex permittivity profiles," Phys. Rev. A **94**(6), 063810 (2016).
47. C. G. King, S. A. R. Horsley, and T. G. Philbin, "Perfect transmission through disordered media," Phys. Rev. Lett. **118**(16), 163201 (2017).
48. S. Longhi, "Kramers-Kronig potentials for the discrete Schrödinger equation," Phys. Rev. A **96**(4), 042106 (2017).
49. S. Longhi, "Reflectionless and invisible potentials in photonic lattices," Opt. Lett. **42**(16), 3229–3232 (2017).
50. C. G. King, S. A. R. Horsley, and T. G. Philbin, "Zero reflection and transmission in graded index media," J. Opt. **19**(8), 085603 (2017).
51. K. G. Makris, I. Krešić, A. Brandstötter, and S. Rotter, "Scattering-free channels of invisibility across non-Hermitian media," Optica **7**(6), 619–623 (2020).
52. D. Liu, Y. Huang, H. Hu, L. Liu, D. Gao, L. Ran, D. Ye, and Y. Luo, "Designing spatial Kramers–Kronig media using transformation optics," IEEE Trans. Antennas Propag. **68**(4), 2945–2949 (2020).
53. N. Radwell, T. W. Clark, B. Piccirillo, S. M. Barnett, and S. Franke-Arnold, "Spatially dependent electromagnetically induced transparency," Phys. Rev. Lett. **114**(12), 123603 (2015).
54. S. Sharma and T. N. Dey, "Phase-induced transparency-mediated structured-beam generation in a closed-loop tripod configuration," Phys. Rev. A **96**(3), 033811 (2017).
55. H. R. Hamedi, V. Kudriašov, J. Ruseckas, and G. Juzel unas, "Azimuthal modulation of electromagnetically induced transparency using structured light," Opt. Express **26**(22), 28249–28262 (2018).
56. L. D. Landau and E. M. Lifshitz, *Electrodynamics of continuous media* (Butterworth-Heinemann, 2004).
57. M. Born and E. Wolf, *Principles of optics* (Cambridge University Press, 1980), 6th ed.
58. M. Artoni, G. La Rocca, and F. Bassani, "Resonantly absorbing one-dimensional photonic crystals," Phys. Rev. E **72**(4), 046604 (2005).
59. Y. Zhang, Y. Xue, G. Wang, C.-L. Cui, R. Wang, and J.-H. Wu, "Steady optical spectra and light propagation dynamics in cold atomic samples with homogeneous or inhomogeneous densities," Opt. Express **19**(3), 2111–2119 (2011).
60. R. Folman, P. Kruger, D. Cassettari, B. Hessmo, T. Maier, and J. Schmiedmayer, "Controlling cold atoms using nanofabricated surfaces: atom chips," Phys. Rev. Lett. **84**(20), 4749–4752 (2000).
61. M. F. Riedel, P. Bohi, Y. Li, T. W. Hansch, A. Sinatra, and P. Treutlein, "Atom-chip-based generation of entanglement for quantum metrology," Nature **464**(7292), 1170–1173 (2010).
62. J. D. Carter and J. D. D. Martin, "Coherent manipulation of cold Rydberg atoms near the surface of an atom chip," Phys. Rev. A **88**(4), 043429 (2013).
63. H. Hattermann, D. Bothner, L. Y. Ley, B. Ferdinand, D. Wiedmaier, L. Sarkany, R. Kleiner, D. Koelle, and J. Fortagh, "Coupling ultracold atoms to a superconducting coplanar waveguide resonator," Nat. Commun. **8**(1), 2254 (2017).